CSIRO PUBLISHING

www.publish.csiro.au/journals/ijwf *International Journal of Wildland Fire* **2010**, *19*, 171–178

An examination of flame shape related to convection heat transfer in deep-fuel beds

Kara M. Yedinak[A,B,*], *Jack D. Cohen*[A,C,*], *Jason M. Forthofer*[A] *and Mark A. Finney*[A]

[A]USDA Forest Service, Rocky Mountain Research Station, Missoula, MT 59808, USA.
[B]Laboratory of Atmospheric Research, Washington State University, Pullman, WA 99163, USA.
[C]Corresponding author. Email: jcohen@fs.fed.us
*Authors have contributed equally to this paper.

Abstract. Fire spread through a fuel bed produces an observable curved combustion interface. This shape has been schematically represented largely without consideration for fire spread processes. The shape and dynamics of the flame profile within the fuel bed likely reflect the mechanisms of heat transfer necessary for the pre-heating and ignition of the fuel during fire spread. We developed a simple laminar flame model for examining convection heat transfer as a potentially significant fire spread process. The flame model produced a flame profile qualitatively comparable to experimental flames and similar to the combustion interface of spreading fires. The model comparison to flame experiments revealed that at increasing fuel depths (>0.7 m), lateral flame extension was increased through transition and turbulent flame behaviour. Given previous research indicating that radiation is not sufficient for fire spread, this research suggests that flame turbulence can produce the convection heat transfer (i.e. flame contact) necessary for fire spread particularly in vertically arranged, discontinuous fuels such as shrub and tree canopies.

Additional keywords: crown fires, discontinuous fuels, laminar flame model, wildfire convection heat transfer.

Introduction

A propagating fire produces a combustion interface between burning and preheating fuel. This curved interface has been characterised schematically in shallow, continuous fuel beds with little attention given as to how the resulting interface geometry relates to fire spread (e.g. Fons 1946; Albini 1967; Frandsen 1971; Rothermel 1972). Previous research has assumed that radiation is exclusively responsible for fire spread and qualitatively described the interface as a planar steady surface (Albini 1982) or solved for it numerically as a steady boundary (Albini 1985, 1986, 1996; Catchpole *et al*. 2002). For fuel beds having significant gaps between fuel elements (discontinuous fuel beds), other research suggests that convection heat transfer (flame contact) in addition to radiation is necessary for fire spread and is related to the combustion interface (i.e. flame) dynamics (Vogel and Williams 1970; Weber 1990; Beer 1995; Finney *et al*. 2006).

Convection heat transfer has been little studied although research suggests it may be necessary for fire propagation. Hottel *et al*. (1965) could not determine that fire spread was principally caused by radiation and proposed a model for convection preheating by horizontal flame 'excursions' into unburned fuel. Based on laboratory experiments using dead surface fuels, Anderson (1969) found that radiation heat transfer accounted for only 40% of the heat transfer necessary to sustain fire spread. Similarly for tree canopies, Van Wagner (1977) found that radiation provided less than 50% of the required heat transfer during crown fire experiments in pine plantations. This suggests convection as a principal preheating and ignition process. Weber (1990) describes fire spread due to vertically expanding laminar flames that produce flame contact and thus convective heating within the fuel bed. Weber (1991) also reports the inability of various fire spread models to appropriately describe the fuel particle temperature rise (i.e. heat transfer mechanisms) while predicting spread rates. Pitts (1991) cites studies that identify flame contact and convection heat transfer as necessary for the fire spread process. Additionally, laboratory experiments found that flame radiation from above the fuel bed contributes little to fuel preheating (McCarter and Broido 1965; de Mestre *et al*. 1985). These research findings suggest the necessity for convection heating during fire spread with the principal pre-ignition heat transfer occurring within the fuel bed. For this to occur, convection heating (i.e. flame contact) within the fuel bed would require flames to extend across the voids within the fuel bed whether at the scale of surface litter fuels (Anderson 1969) or live tree canopies (Van Wagner 1977).

Commonly, fire spread models have assumed steady spread (Rothermel 1972; Albini 1985, 1986, 1996; Catchpole *et al*. 2002). However, the non-steady heating and ignition processes at the scale of fuel particles implies that this common 'quasi-steady' fire spread assumption (Berlad 1970) applies only as an ensemble average across some broader scales of time and distance. Fuel particles and voids comprise the fuel bed and fire spreads

 10.1071/WF07143 1049-8001/10/020171

within the fuel bed as discontinuous, non-steady advances. Non-steady flames contact adjacent fuel particles and ignitions occur across fuel voids. Thus, a 'quasi-steady' fire spread model may have to account for the non-steady processes to appropriately produce the 'quasi-steady' behaviour. This suggests consideration for convection heating within the fuel bed as a significant fire spread process.

The geometry and dynamics of the flame determines whether or not flame contact will occur with adjacent unburned fuel, resulting in fire spread. Weber (1990) developed a model for small vertical match-stick fuel elements that assumed a laminar flame that expands with height. This model was useful in understanding the observed flame contact required for fire propagation through an array of discontinuous fuel elements (Vogel and Williams 1970; Weber 1990). Emmons (1965) noted that the total geometry of the flame-fuel system determines the flame propagation. These independent studies place importance on the geometry of the flame as it relates to heat transfer mechanisms and flame propagation.

Our study examines flame profiles using a simple flame model compared with experiments. The model characterises a laminar flame profile that results solely from the generation of combustion products and buoyancy acting on those hot gases. We developed this simple flame model solely as a means for exploring flame expansion and to examine the potential for convection heating. The model is not intended for fire spread prediction. Rather, we developed this simple flame model in conjunction with experiments as a means for examining the potential for convection heating as a fire spread process. Assumptions in the model produce the maximum possible lateral laminar flame expansion. Simple burning experiments using three different vertical fuel heights were conducted for comparison with the laminar flame model results.

Methods

Laminar flame model

Assumptions

We developed a model for a single vertical fuel source. The following simplifying assumptions (particularly 1, 3 and 5) were purposefully chosen to overestimate the laminar flame expansion around the fuel source. The vertical fuel source is considered a solid cylinder with the combustion reaction occurring at the surface of the vertically continuous fuel column (Fig. 1). The model assumes the following: the flame fluid generation is (1) from a complete stoichiometric reaction occurring instantaneously at a (2) constant and uniform rate with fuel height. The flame fluid is (3) an ideal gas (4) equivalent to air with (5) constant uniform temperature and ambient pressure. The combustion products (hot gases) (6) have no initial velocity, (7) are only affected by buoyant forces that produce a (8) one dimensional, (9) steady-state, (10) irrotational and (11) inviscid flow. The (12) flame forms externally to and uniformly around the solid fuel. Flame behaviour adjacent to the fuel is not influenced by the (13) above-fuel flame and (14) ambient air.

We assumed that the combustion is complete and the reaction time is negligible compared with the flame flow. Thus, we related the fuel mass loss rate (experimentally measured) to the flame by assuming that an instantaneous and complete stoichiometric

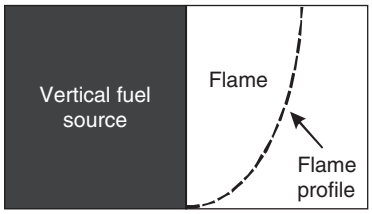

Fig. 1. A conceptual laminar flame profile developing from the surface of a cylindrical, vertical fuel source is shown. The combustion reaction occurs completely at the solid surface resulting in the combustion products forming the 'flame' profile.

chemical reaction (with air) occurs uniformly along the fuel's vertical extent (assumptions 1 and 2). We represented the dry excelsior fuel with an empirical formula based on an ultimate chemical analysis of poplar (*Populus* sp.) wood (Tillman *et al.* 1981). The following is the stoichiometric combustion equation for the dry wood:

$$C_{4.30}H_{6.30}O_{2.59} + 4.58(O_2 + 3.76\,N_2) \rightarrow 4.30\,CO_2 + 3.15\,H_2O + 4.58(3.76\,N_2) \quad (1)$$

The gases on the equation's right hand side comprise the flame and thus the flame mass. The flame : fuel mass ratio is 7.33 (e.g. 1 g of fuel yields 7.33 g of flame). The solid fuel mass loss rate (experimentally measured) multiplied by the flame : fuel mass ratio determines the flame mass flow rate (value of C in Eqn 5).

We assumed that the flame behaves as an ideal gas at the constant uniform temperature and pressure of 1000 K and 9.01×10^4 Pa (ambient during experiments) respectively (assumptions 3 and 5). Analysis at this temperature and pressure reveals that each constituent flame gas from the above chemical equation has a compressibility factor of $\sim$1.0 indicating ideal gas behaviour (Black and Hartley 1985).

We assumed that the flame has the properties of air (assumption 4). The computed flame gram molecular weight of 29.5 g mole^{-1} results in a gas constant of 281.8 J kg^{-1} K^{-1}. This gas constant is less than 2% different from that of air and thus we used the properties of air for the flame model calculations.

The remaining assumptions (6–14) simplify the dynamics, characterise the flow as laminar and simplify the fuel and environmental conditions. Assumption 6 designates that the combustion products are generated from a zero-velocity surface and thus initially have zero velocity. In conjunction with assumptions 1, 3, 4 and 5, we assumed that the expansion time of the combustion products is negligible compared with the flame flow. We thereby assumed that the combustion gases instantaneously expand and mix with the upward flame flow (above the zero fuel height) to a volume where the flame pressure equals the ambient pressure. The combustion gases accelerate upwards to produce a vertical flow due to buoyant forces (assumptions 7 and 8). The assumed uniform conditions (assumptions 2 and 5) result in steady-state (assumption 9) laminar flow (assumptions 10 and 11). Any solid wood fuel within the flame volume is considered negligible (assumption 12). Consistent with this assumption, during the experimental phase, we wrapped the excelsior fuel densely on the supporting rods such that burning principally occurred at the bulk fuel surface during the

experimental measurements. We assumed no convective flow restrictions above the flame (assumption 13) and no cross flows (assumption 14). In accordance with these assumptions, we conducted the experiments at the Missoula Fire Sciences Laboratory combustion facility under no-wind conditions.

Numerical solution

Given the above assumptions, the shape of the flame profile is determined by the conservation of mass and momentum related to the changes in mass and velocity of the gasses in the flame. Thus, the net forces acting on the flame fluid are equal to the net change in momentum of the fluid. This relationship can be written as:

$$\frac{d(mw)}{dz} = F'_{z,net} \tag{2}$$

where m is the mass flux through the flame cross-sectional area at height z, w is the velocity of the flame fluid at z, and $F'_{z,net}$ is the net force due to gravity acting on density differences per unit length along the z-axis. The net force expression is related to the density of ambient air (ρ_a), the density of the flame (ρ_f), gravitational acceleration (g) and the flame fluid cross-sectional area (A):

$$F'_{z,net} = Ag(\rho_a - \rho_f) \tag{3}$$

Substituting (3) into (2) yields:

$$\frac{d(mw)}{dz} = Ag(\rho_a - \rho_f) \tag{4}$$

We derived the second expression from the mass flow rate term. To meet the assumptions of steady-state and laminar, the total amount of flame mass issuing from the vertical source must equal the total amount of mass leaving the cross-sectional area at the final height. This can be expressed as:

$$\dot{m} = Cz = \rho_f Aw \tag{5}$$

where C is the flame mass generated per unit time per unit length at height z. From the model assumptions, the flame mass C is the solid fuel mass loss rate times the flame : fuel mass ratio determined above (Eqn 1). For the purpose of numerically solving the ordinary differential equation that results from combining (4) and (5), let:

$$y_1 = \rho_f Aw^2 \tag{6}$$

$$y_2 = \rho_f Aw \tag{7}$$

By solving Eqns 6 and 7 for A, and then substituting this into Eqn 4, it becomes:

$$\frac{dy_1}{dz} = -g(\rho_f - \rho_a)\frac{y_2^2}{\rho_f y_1} \tag{8}$$

where all the variables are in terms of y_1 and y_2. By substituting Eqn 7 into Eqn 5 and for C constant with height z (assumption 2), the derivative with respect to z of Eqn 5 becomes:

$$\frac{dy_2}{dz} = C \tag{9}$$

Using a fourth-order Runge–Kutta numerical method, we solve for y_1 and y_2 and are then able to use these values to obtain w and A at each z-height interval (0.0001 m). We verified that these results were independent of the grid and numerical solver.

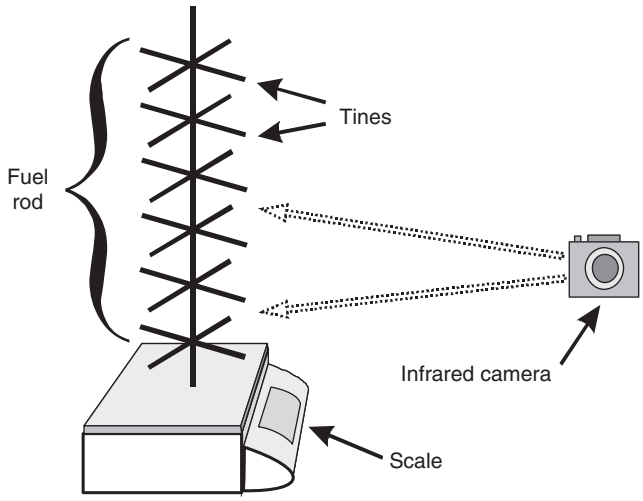

Fig. 2. The excelsior fuel rod experiments consisted of a scale supported upright steel fuel rod with perpendicular cross tines used to hold vertically arranged excelsior. The flame produced by burning excelsior is sampled with an infrared camera at 120 Hz.

Laboratory burn experiments

We conducted experiments to examine the extent of flame expansion from a woody fuel source under no-wind conditions. The fuel source consisted of a vertical steel rod wrapped with excelsior (shredded *Populus* sp. wood). The excelsior was held in place by perpendicular wire cross tines attached to the rod at intervals of 7.5 cm and the rod was mounted on an electronic balance (Fig. 2). The experiments included three heights of excelsior (30, 60 and 120 cm) with a fuel loading of 250 g m^{-1}. For the 30-, 60- and 120-cm fuel rod heights, four, five and four replications were conducted respectively. Mass loss data were collected directly from the balance at intervals of 0.5 s for the full duration of the burning experiment.

The combustion process was defined by the stoichiometric equation (Eqn 1) and thus the combustion rate was determined by measuring the fuel mass loss. Each excelsior fuel rod was ignited by spraying ethyl alcohol over the entire outer surface to ensure simultaneous ignition over the full height of the excelsior. The mass loss data during the ignition phase of alcohol burning was not used and identified as the Phase I burning rate (Fig. 3). To determine the mass loss or burning rate of the excelsior, the data were examined to find the period for which the alcohol had burned off but the fuel rod was still burning along the full height of the fuel. This period was initially determined by using real-time mass loss readings. The interval was further refined by examination of the resulting digital still images. The resulting 8-s interval was then verified with the mass loss data to ensure that the region had a relatively constant slope; i.e. a uniform mass loss rate (Fig. 3, Phase II). The 8-s sample interval resulted in 17 fuel mass measurements.

An overall mass loss rate designated for each fuel height was calculated based on the respective mass loss data. A centred, 1-s interval (0.5-s sample) mass loss computation provided 15 1-s average mass loss rates per burn experiment. The average and standard deviation for each fuel height (30, 60 and 120 cm) were

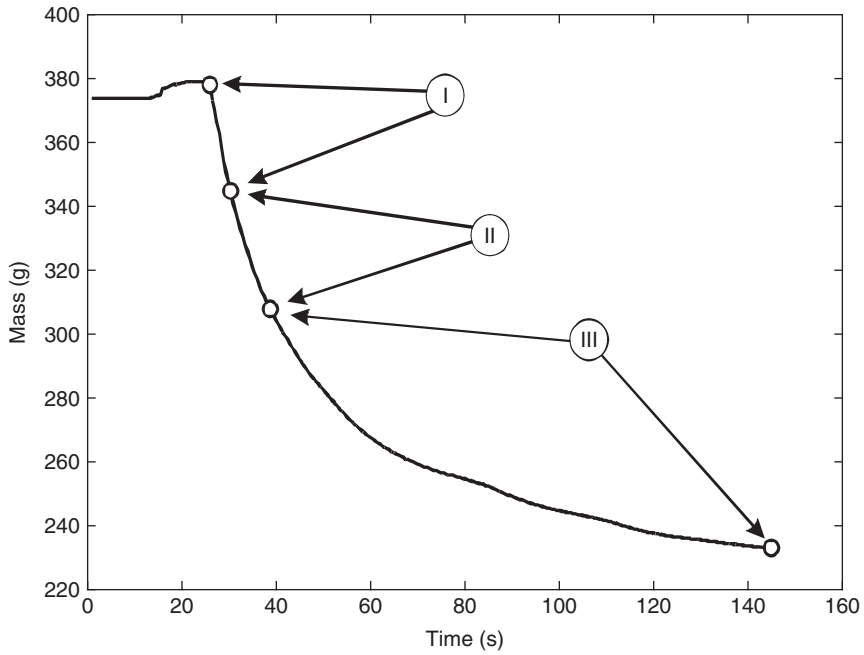

Fig. 3. Three main periods of burning can be identified in the mass loss data. Phase I is where ethyl alcohol is burned off. Phase II represents consistent external burning of the excelsior at a constant rate following complete combustion of the ethyl alcohol (constant slope). Phase III represents significant excelsior consumption where the excelsior fuel volume is decreasing and the interface between the excelsior and flame is no longer a vertical line.

calculated using all the 1-s mass loss rates from their respective fuel height burning experiments. The average and two standard deviations ($\pm 2\sigma$) mass loss rates for each fuel height were used as inputs for the flame mass generation rates (C, Eqn 9) used in the laminar flame model.

Model comparisons with the experimental flame profiles used digital infrared imaging. The experimental flame shapes were captured with an infrared (3–5-μm range) camera (TVS-8500, Cincinnati Electronics, Mason, OH) during the burning process. The infrared camera sampled 120 frames s^{-1} for ~8 s. The resulting 1024 frames of digital infrared data were analysed for flame presence or absence. Flames were considered present in a pixel for a specific frame if the blackbody equivalent temperature for that pixel was ≥823 K. Using the presence and absence data for all frames, an occurrence frequency of flame presence was constructed with respect to flame position.

Results

The burn experiments provided not only actual flame profiles but also the corresponding fuel mass loss. The average and standard deviation of measured combustion mass loss rates for each fuel height (Table 1) determine the flame mass generation rates (C) used to model the flame profile for each of the fuel heights. Fig. 4*b* shows the modelled flame profile for the average mass loss rate (solid line) and the profiles for $\pm 2\sigma$ mass loss rates (dashed lines).

The corresponding infrared images display the occurrence frequencies of flame presence with respect to the lateral flame extension from the fuel (Fig. 4*c*). The occurrence frequencies are represented spatially with contour lines for each 10% frequency of flame presence during the sampled burning period. The frequencies of occurrence range from 100% where the flame always occurs to 0% where no flame is observed.

Table 1. Mass loss rates for excelsior fuel rod burning experiments
The average mass loss rates and $+2\sigma$ were calculated using a total of 60, 75 and 60 1-s intervals for the 30-, 60- and 120-cm fuel heights respectively. These values were used as the mass loss rates that determine the flame mass (C), an input to the laminar flame model

Fuel height (cm)	Average mass-loss rate ($g\,m^{-1}\,s^{-1}$)	Two standard deviations ($g\,m^{-1}\,s^{-1}$)
30	5.92	2.00
60	7.03	1.98
120	6.07	2.69

The lateral flame expansions during the experimental fires provide a quantitative comparison with the modelled flame (Table 2). The maximum lateral flame extension at the top fuel height was used for the comparison with the modelled flame. The thermal image expansion distances correspond to the occurrence frequencies (>50, >10%) of flame presence. A comparison of the modelled flame with the actual flame expansion reveals the anticipated model overestimate for the 30-cm fuel height. However, inspection of the data reveals that this overestimation reduces with increased fuel height and significantly at the 10% contour.

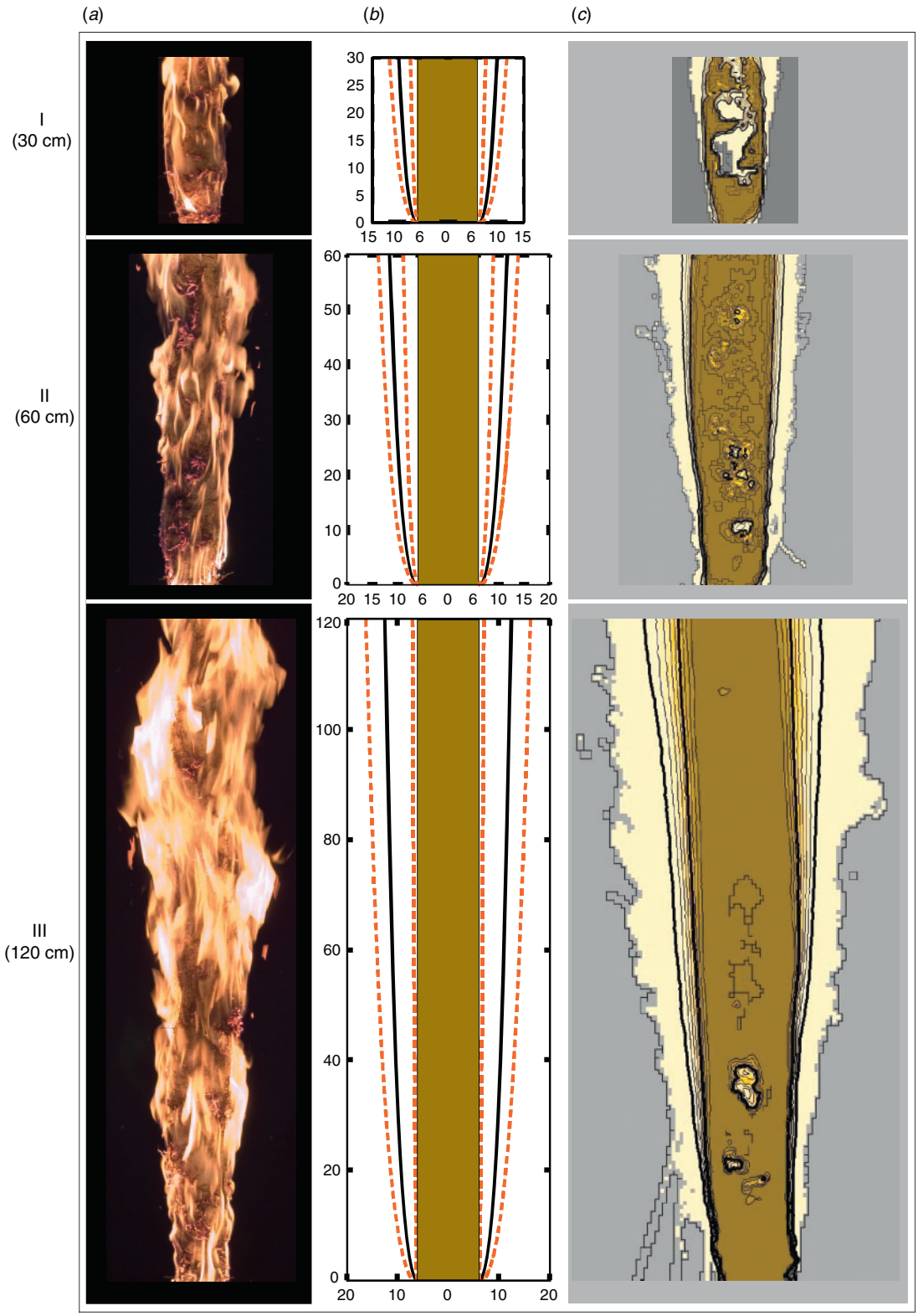

Fig. 4. Visible photographs of the 30, 60 and 120 cm tall excelsior fuel rods with an undulating flame edge indicating non-steady flame behaviour (*a*). Numerical solution for a 30, 60 and 120 cm-tall excelsior fuel rod having average mass loss rates of 5.92, 7.03 and 6.07 g m^{-1} s^{-1} respectively (*b*). The fuel is represented by the solid rectangle in the centre (spanning the horizontal distance −6.0 to 6.0 cm). The solid and dashed lines to either side of the fuel are the model results representing the mass-loss rate average (solid line) and $\pm 2\sigma$ of that average (dashed lines). The frequency of flame presence is based on a radiant temperature threshold of 823 K (*c*). Contour lines are in 10% increments that outwardly decrease. The 50 and 10% presence contours are shown with heavier lines.

Table 2. Modelled and measured flame expansion

The amount of over-estimation in the laminar flame model decreases with height, compared with the experimental flame expansion. At 30 cm, the modelled distance from fuel surface is quite large as compared with the experimental values. However, at 120 cm, the modelled distance from the fuel surface at $+2\sigma$ mass loss rate is within the experimentally measured 10% flame occurrence

Fuel height (cm)	Modelled flame edge distance from fuel surface (cm)		Experimentally measured flame edge distance from fuel surface at frequency of occurrence (cm)	
	Average	Average $+ 2\sigma$	50%	10%
30	3.35	5.33	1.01	2.27
60	5.75	7.99	2.54	6.41
120	6.68	10.47	3.66	10.49

The frequency contours suggest non-steady flame behaviour. The contours produce a smooth time averaged flame edge at frequencies of 10% and higher, but jagged at frequencies less than 10%. This implies a non-steady flame edge that can also be inferred from the photographs taken during the burning experiment (Fig. 4*a*). Further inspection of these photographs indicates that the non-steady behaviour increases above the 30–60-cm height. This suggests a changing flow regime (i.e. turbulence) that laterally extends the flame position (Fig. 4*c*).

Discussion

Our study expands upon Weber's (1990) research that showed how flame expansion could span fuel voids to contact and ignite adjacent fuel elements. Whereas Weber (1990) used a derived mathematical function to define the flame profile, we determined the flame profile with a numerically solved physical flame model. Our study qualitatively concurs with Weber (1990) regarding the potential importance of flame expansion within the fuel bed to produce flame contact with adjoining fuels and thus convection heat transfer for fire spread.

Laminar flame model compared with experiments

A comparison of the modelled flame with the actual flame expansion reveals qualitatively similar flame shapes. As anticipated, we found the model to over-estimate for the 30-cm fuel height. However, the over-estimate diminished with height; i.e. at 60 and 120 cm. Inspection of the thermal image flame frequencies (Fig. 4*c*) and digital photographs (Fig. 4*a*) reveal non-steady flame behaviour not captured by our laminar flame model. Fig. 4*c* reveals that frequencies of 10% and higher produce smooth time averaged flame contours; however, the jagged outer contour (0–10% frequency) displays non-steady flame behaviour. This implies a non-steady flame edge that can also be observed in the photographs taken during the burning experiment (Fig. 4*a*). The increasing lateral expansion of the 0–10% flame frequencies greater than 30 cm (Fig. 4*c*) also indicates increasing non-steady flame behaviour.

Inspection of the data (Table 2) reveals that even though the profile shapes remain qualitatively similar, the over-estimation in lateral expansion reduces with increased fuel height at the 10% contour (Fig. 4*c*). This suggests a change in flow dynamics at greater fuel heights. That is, the over-estimating model assumptions largely account for the dominant processes affecting flame expansion at the 30-cm fuel height. However, at greater heights, unaccounted factors become important. The model assumes that the mass generation and the buoyant force solely determine the flame profile without consideration for viscous forces. The reduced model over-estimation with height compared with the experimental flame profiles suggests that unaccounted viscous influences could result in increased flame expansion.

Flame turbulence

The simplifying assumptions of the flame model neglect any viscous influences (assumptions 7, 10 and 11) and thus the model does not consider the onset of transition and turbulent flow. The occurrence of transition and turbulence would be consistent with the changing relationship between the modelled flame profile and the actual flame behaviour. We calculated the Grashof number to diagnostically examine the likelihood of turbulent flames.

A Grashof number analysis of the experimental flames as natural convection indicates that transition and turbulence can be expected for the 60- and 120-cm fuel heights. The Grashof number is a dimensionless quantity that is correlated with the flow condition (laminar, transition and turbulent) of natural convection (buoyantly induced flow). We calculate the Grashof number using the ambient conditions present during the burning experiments and those assumed in the model (see *Appendix*). This calculation indicates turbulent flow of the experimental flames at heights greater than 70 cm (Incopera and DeWitt 2002; Quintiere 2006). Thus, turbulence and the transition to turbulence are what likely influence the flame expansion at the top of the 60-cm fuel and nearly one-half of the 120-cm fuel.

Our analysis indicates the possibility for convection heat transfer due to turbulent flames in discontinuous vertically arranged fuels deeper than 0.7 m. This is supported by the laboratory experiments by Finney *et al*. (2006) that report fire spread in discontinuous fuels only after the occurrence of flame contact across the fuel voids. Flame turbulence provides the physical mechanism for the flame 'excursions' suggested by Hottel *et al*. (1965) and observed by Finney *et al*. (2006). The turbulence increases the potential for flames to extend across voids and ignite unburned fuel by convective heat transfer.

Conclusions

We used a simple flame model for examining flame behaviour rather than for actual flame representation. Although the model produced flame profiles qualitatively similar to the profiles of

experimental flames, our model assumptions were intended to produce a steady flame boundary that overestimated the flame expansion. The experiments revealed non-steady flames and the model over-estimation diminished at heights greater than 30 cm. The observed non-steady behaviour and flame expansion of the experiments suggest turbulence as a potential mechanism for convection heating within a vertically arranged, discontinuous fuel bed. Using the thermal image 10% flame occurrence contour (Fig. 4*c*), the model over-estimate (Fig. 4*b*) declined at 60 cm and no over-estimate occurred at the 120-cm fuel height. Measurements of the experimental fires revealed non-steady flame behaviour at 60 cm and higher that indicated the onset of transition and turbulent flow. A diagnostic analysis using the Grashof number indicated turbulence at fuel depths greater than 0.70 m that concurred with the observations. Thus, we found through observation and measurement that non-steady flames can increase the lateral expansion of the flame profile within the fuel bed. Further, our analysis identified flame turbulence as a mechanism by which convection heat transfer can occur within deep (>70 cm), vertically arranged, discontinuous fuel beds.

Acknowledgements

We thank Ian Grob, Anita Hershman, Danielle Paige, Isaac Grenfell, Kyle Shannon and James Riser for their technical support in the development of this research.

References

Albini FA (1967) A physical model for firespread in brush. In '11th Symposium on Combustion', 14–20 August 1966, Berkeley, CA. pp. 553–560. (The Combustion Institute: Pittsburgh, PA)

Albini FA (1982) Response of free-burning fires to non-steady wind. *Combustion Science and Technology* **29**, 225–241. doi:10.1080/00102208208923599

Albini FA (1985) A model for fire spread in wildland fuels by radiation. *Combustion Science and Technology* **42**, 229–258. doi:10.1080/00102208508960381

Albini FA (1986) Wildland fire spread by radiation – a model including fuel cooling by natural convection. *Combustion Science and Technology* **45**, 101–113. doi:10.1080/00102208608923844

Albini FA (1996) Iterative solution of the radiation transport equations governing spread of fire in wildland fuel. *Combustion, Explosion, and Shock Waves* **32**, 534–543. doi:10.1007/BF01998575

Anderson HE (1969) Heat transfer and fire spread. USDA Forest Service, Intermountain Forest and Range Experiment Station, Research Paper INT-RP-69. (Ogden, UT)

Beer T (1995) Fire propagation in vertical stick arrays: the effects of wind. *International Journal of Wildland Fire* **5**, 43–49. doi:10.1071/WF9950043

Berlad AL (1970) Fire spread in solid fuel arrays. *Combustion and Flame* **14**, 123–136. doi:10.1016/S0010-2180(70)80018-9

Black WZ, Hartley JG (1985) 'Thermodynamics.' (Harper and Row: New York)

Catchpole WR, Catchpole EA, Tate AG, Butler B, Rothermel RC (2002) A model for the steady spread of fire through a homogeneous fuel bed. In 'Forest Fire Research and Wildland Fire Safety: Proceedings of IV International Conference on Forest Fire Research', 18–23 November 2002, Luso, Coimbra, Portugal. (Ed. DX Viegas) (Millpress: Rotterdam, the Netherlands)

de Mestre N, Rothermel RC, Wilson R, Albini F (1985) Radiation screened fire propagation. University of New South Wales, University College ADFA, Report No. 2/85. (Canberra)

Emmons HW (1965) Fundamental problems of the free burning fire. In '10th Symposium (International) on Combustion', 17–21 August 1964, Cambridge, UK. pp. 951–964. (The Combustion Institute: Pittsburgh, PA)

Finney MA, Cohen JD, Grenfell IC, Yedinak KM (2006) Experiments on fire spread in discontinuous fuelbeds. In 'V International Conference on Forest Fire Research', 27–30 November 2006, Figuiera de Foz, Coimbra, Portugal. (Ed. DX Viegas) (CD-ROM) (Elsevier)

Fons WL (1946) Analysis of fire spread in light forest fuels. *Journal of Agricultural Research* **72**, 93–120.

Frandsen WH (1971) Fire spread through porous fuels from the conservation of energy. *Combustion and Flame* **16**, 9–16. doi:10.1016/S0010-2180(71)80005-6

Hottel HC, Williams GC, Steward FR (1965) The modelling of firespread through a fuel bed. In '10th Symposium (International) on Combustion', 17–21 August 1964, Cambridge, UK. pp. 997–1007. (The Combustion Institute: Pittsburgh, PA)

Incopera FP, DeWitt DP (2002) 'Fundamentals of heat and mass transfer.' 5th edn. (Wiley: New York)

McCarter RJ, Broido A (1965) Radiative and convective energy from wood crib fires. *Pyrodynamics* **2**, 65–85.

Pitts WM (1991) Wind effects on fires. *Progress in Energy and Combustion Science* **17**, 83–134. doi:10.1016/0360-1285(91)90017-H

Quintiere JG (2006) 'Fundamentals of fire phenomena.' (Wiley: New York)

Rothermel RC (1972) A mathematical model for predicting fire spread in wildland fuels. USDA Forest Service, Intermountain Forest and Range Experiment Station Research Paper INT-115. (Ogden, UT)

Tillman DA, Rossi AJ, Kitto WD (1981) 'Wood combustion: principles, processes, and economics.' (Academic Press: New York)

Van Wagner CE (1977) Conditions for the start and spread of crown fire. *Canadian Journal of Forest Research* **7**, 23–34. doi:10.1139/X77-004

Vogel M, Williams FA (1970) Flame propagation along matchstick arrays. *Combustion Science and Technology* **1**, 429–436. doi:10.1080/00102206908952223

Weber RO (1990) A model for fire propagation in arrays. *Mathematical and Computer Modelling* **13**, 95–102. doi:10.1016/0895-7177(90)90103-T

Weber RO (1991) Modelling fire spread through fuel beds. *Progress in Energy and Combustion Science* **17**, 67–82. doi:10.1016/0360-1285(91)90003-6

Manuscript received 29 September 2007, accepted 15 August 2008

Appendix

Eqn A1 represents the Grashof number.

$$Gr = \frac{\beta g(T_{flame} - T_{\infty})l^3}{\upsilon_{film}^2} \quad \text{(A1)}$$

A Grashof number value of $Gr \geq 10^9$ indicates turbulent natural convection (Quintiere 2006). By setting $Gr = 10^9$ and solving for the flow length, l we can estimate the flame height at which turbulent flow is expected:

$$l = \left(\frac{1 \times 10^9 (\upsilon_{film}^2)}{\beta g(T_{flame} - T_{\infty})} \right)^{1/3} \quad \text{(A2)}$$

where $T_{flame} = 1000\,\text{K}$; $T_{\infty} = 294\,\text{K}$; $T_{film} = (T_{flame} + T_{\infty})/2 = 647\,\text{K}$; $g = 9.81\,\text{m s}^{-2}$; β, fluid expansion coefficient; for an ideal gas, $\beta \approx 1/T_{film} = 1.48 \times 10^{-3}\,\text{K}^{-1}$; ν_{film}, kinematic viscosity; $\nu_{film}(T_{film}) = 59.76 \times 10^{-6}\,\text{m}^2\,\text{s}^{-1}$ (A4; Incopera and DeWitt 2002); $l = 0.694\,\text{m}$ (flow length).

The Grashof number analysis indicates that we should expect turbulent flame convection at lengths of 0.7 m and greater.